First-principles study of the magnetic interactions in honeycomb Na_2IrO_3

Y. S. Hou,[1,2] J. H. Yang,[3] H. J. Xiang,[1,2,*] and X. G. Gong[1,2,†]

[1]*Key Laboratory of Computational Physical Sciences (Ministry of Education), State Key Laboratory of Surface Physics, Department of Physics, Fudan University, Shanghai 200433, China*

[2]*Collaborative Innovation Center of Advanced Microstructures, Nanjing 210093, China*

[3]*National Renewable Energy Laboratory, Golden, Colorado 80401, USA*

(Received 7 August 2017; revised manuscript received 20 July 2018; published 4 September 2018)

Honeycomb iridate Na_2IrO_3, a $J_{\rm eff} = 1/2$ magnet, is a potential platform for realizing quantum spin liquid. Many experiments have shown that its magnetic ground state is a zigzag antiferromagnetic order. However, there is still a lack of consensus on the theoretical model explaining such order, since its second-nearest-neighbor (NN) and long-range third-NN magnetic interactions are highly unclear. By properly considering the orbital moments achieved through constraining their directions in first-principles calculations, we obtain that the relative angle between orbital and spin moments is fairly small and in the order of several degrees, which thus validates the $J_{\rm eff} = 1/2$ state in Na_2IrO_3. Surprisingly, we find that the long-range third-NN Heisenberg interactions are sizable, whereas the second-NN magnetic interactions are negligible. Furthermore, we show that sizable long-range third-NN Heisenberg interactions closely correlate with the appreciable distribution of Wannier orbitals of $J_{\rm eff} = 1/2$ states over the three NN Ir atoms. Based on our study, we propose a minimal J_1-K_1-Γ_1-J_3 model in which the magnetic excitations have an intensity peak at 5.6 meV, consistent with the inelastic neutron-scattering experiment [Phys. Rev. Lett. **108**, 127204 (2012)]. The present work demonstrates again that constraining orbital moments in first-principles calculations is a powerful way to investigate the intriguing magnetism in $J_{\rm eff} = 1/2$ magnets, and it paves the way toward gaining a deep insight into the novel magnetism discovered in the honeycomb $J_{\rm eff} = 1/2$ magnets.

DOI: 10.1103/PhysRevB.98.094401

I. INTRODUCTION

Recently, iridium oxides had been increasingly studied both experimentally and theoretically. Many novel and intriguing phenomena have been put forward [1], such as topological Mott insulators [2], Weyl semimetal and axion insulators [3], unconventional high-temperature superconductivity [4,5], etc. Among the iridium oxides, the honeycomb A_2IrO_3 (A = Li,Na) are of particular interest because it has been theoretically predicted [6,7] that they could realize the long-sought Kitaev model, which has an exactly solvable quantum spin-liquid ground state [8]. Many experimental studies on these iridium oxides have also been inspired to discover the exotic and interesting quantum spin liquid [9–14].

Experimentally, it has been shown that the prototypical honeycomb iridium oxide Na_2IrO_3 has a zigzag antiferromagnetic (AFM) order, and its magnetic easy axis is approximately halfway between the cubic $\boldsymbol{x}$- and $\boldsymbol{y}$-axes [9,10,14,15]. Theoretically, a general consensus among the models explaining such order is still lacking, and there exist many diverse models [7,11,12,16–24]. The most controversial issue focuses on the second- and third-nearest-neighbor (NN) magnetic interactions. First, models consisting of only the NN interactions are proposed to give rise to the zigzag AFM order [7,17,21], whereas it is urged that the second- and third-NN magnetic interactions should also be taken into account [11,12,18–20]. Secondly, the types and strengths of the second- and third-NN magnetic interactions are strikingly disputed. Kimchi *et al.* proposed that the zigzag AFM order could be explained by the Heisenberg-Kitaev model only plus the second- and third-NN Heisenberg interactions (HK-J_1-J_2 model) [18], but the second-NN Kitaev interaction is also argued to be important [19]. As for their strength, fitting the HK-J_1-J_2 model to the experimentally measured spin wave shows $J_2/J_1 = 0.78$ and $J_3/J_1 = 0.9$ [11], but theoretical calculations using nonperturbative exact diagonalization methods demonstrate that the long-range third-NN Heisenberg interaction J_3 is unexpectedly strong while both the NN Heisenberg interaction J_1 and the second-NN Heisenberg interaction J_2 are negligible [20]. These results are elusive because the bond distances of both the second- and third-NN Ir-Ir pairs are nearly two times longer than those of the NN Ir-Ir pairs.

To gain a deeper insight into the zigzag AFM order in Na_2IrO_3, the key is to determine the magnetic interactions fully, especially the disputed second NN and the long-range third NN on the same footing. So far there are only several first-principles calculations that estimated the second- and third-NN magnetic interactions [23,24], although the NN magnetic interactions have been thoroughly investigated by different methods in many previous studies [19,22–25]. An essential difficulty lies in the fact that orbital moments play an important role in determining the magnetic interactions in $J_{\rm eff} = 1/2$ magnets. For Na_2IrO_3, the total magnetic moment ($1\mu_B$) of the $J_{\rm eff} = 1/2$ state is composed of the dominant

*hxiang@fudan.edu.cn
†xggong@fudan.edu.cn

orbital moment ($2/3\mu_B$) and the spin moment ($1/3\mu_B$) [26]. Our previous study showed that the directions of the spin and orbital moments in the $J_{\text{eff}} = 1/2$ magnets, including Na_2IrO_3, α-Li_2IrO_3, and α-$RuCl_3$, will seriously deviate from each other in first-principles calculations if the directions of the orbital moments are not constrained [27]. To extract the magnetic interaction parameters of the $J_{\text{eff}} = 1/2$ magnet, it is necessary to obtain the total energy of magnetic states with the given directions of spin and orbital moments. Therefore, it is crucial to constrain the direction of orbital moments in the $J_{\text{eff}} = 1/2$ magnets. Note that the widely used energy-mapping method, which only accounts for spin, is obviously not applicable here.

In this work, we study the magnetic interactions of the $J_{\text{eff}} = 1/2$ magnet Na_2IrO_3 by combining maximally localized Wannier functions (MLWFs) with our newly developed method [27], which constrains the directions of orbital moments. Apart from the previously well-studied dominant NN magnetic interactions, we find that the long-range third-NN Ir-Ir bonds have sizable AFM Heisenberg interactions, whereas the second-NN Ir-Ir bonds have negligible magnetic interactions. By projecting onto the $J_{\text{eff}} = 1/2$ Wannier orbitals, we show that the third-NN hopping is much stronger than the second-NN hopping, consistent with our calculated magnetic interaction parameters, and that the sizable third-NN Heisenberg interaction J_3 closely correlates with the appreciable distribution of Wannier orbitals of $J_{\text{eff}} = 1/2$ states over the three NN Ir atoms. Based on our calculated results, we propose a minimal J_1-K_1-Γ_1-J_3 model for Na_2IrO_3, which well explains the following experimental observations: (i) Its magnetic excitations have an intensity peak at 5.6 meV, consistent with the inelastic neutron-scattering experiment [11]; (ii) the third-NN AFM Heisenberg interaction J_3 stabilizes the zigzag AFM order; and (iii) the NN symmetric off-diagonal exchange Γ_1 accounts for the experimentally observed magnetic easy axis. The present work not only shows that our newly developed method is a powerful tool to study the magnetism of materials with non-negligible orbital moments, but it also takes a significant step toward understanding the novel magnetism of honeycomb $J_{\text{eff}} = 1/2$ magnets.

II. COMPUTATIONAL METHODS

Our first-principles calculations based on density-functional theory (DFT) are performed within the generalized gradient approximation (GGA) according to the Perdew-Burke-Ernzerhof (PBE) parametrization as implanted in the Vienna *Ab initio* Simulation Package (VASP) [28]. We use the projector-augmented wave (PAW) method [29] and an energy cutoff of 500 eV. To describe the electron correlation associated with the Ir $5d$ electron, we use the rotationally invariant DFT+U method introduced by Liechtenstein [30]. The on-site Coulomb energy $U = 3.0$ eV and the Hund coupling $J_h = 0.6$ eV [15] are adopted in the present work. Because the Ir atom has a strong spin-orbit coupling (SOC) $\xi_{SO} \sim 0.4$ eV [26], SOC is included in our all calculations. We use the experimental monoclinic crystal structure with the space group $C2/m$ [11].

Since Na_2IrO_3 is a $J_{\text{eff}} = 1/2$ magnet [14,16,19,22], we adopt our recently developed methodology that constrains the directions of orbital moments [27] so as to properly take into account the important effects of orbital moments. To gain a deep insight into the magnetic interactions, hopping parameters are extracted from the real-space Hamiltonian matrix elements in the $J_{\text{eff}} = 1/2$ Wannier orbital basis [31,32], which are obtained by employing the VASP2WANNIER90 interface combined with the WANNIER90 tool [33]. To maintain the symmetry of the Wannier functions we utilize one-shot Wannier construction, in which the minimization of Wannier spread is not performed. The magnetic transition temperature of Na_2IrO_3 is estimated by performing efficient parallel tempering Monte Carlo (MC) simulations [34–36]. A $40 \times 20 \times 1$ supercell of the unit cell, which contains 3200 magnetic ions, is used in these MC simulations.

III. RESULTS

In this section, we first demonstrate that the optimal relative angle between orbital and spin moments is fairly small, and then we confirm by means of our newly developed method that the experimentally observed zigzag AFM structure is truly the magnetic ground state of Na_2IrO_3. Next, we show that the sizable long-range third-NN AFM Heisenberg interaction has its roots in the appreciable distribution of Wannier orbitals of $J_{\text{eff}} = 1/2$ states over the three NN Ir atoms. Lastly, based on our DFT calculated magnetic interaction parameters, we propose a minimal J_1-K_1-Γ_1-J_3 model that well explains experimental observations of Na_2IrO_3.

A. Theoretical reproduction of the zigzag AFM ground state of Na_2IrO_3

Na_2IrO_3 is a layer honeycomb antiferromagnet. It crystallizes in the monoclinic space group $C2/m$ [11] and consists of alternate stacking of $Na_{1/3}Ir_{2/3}O_2$ and Na layers [Fig. 1(a)]. $Na_{1/3}Ir_{2/3}O_2$ layers are composed of edge-sharing IrO_6 octahedrons, and Ir atoms form the honeycomb lattice with Na atoms sitting at the center of the Ir_6 hexagon. It has been experimentally shown that Na_2IrO_3 has a zigzag AFM order [Fig. 1(b)] below 18.1 K [10] and that its magnetic easy axis is approximately along the [110] direction in the ($\boldsymbol{x}$, $\boldsymbol{y}$, $\boldsymbol{z}$) coordinates whose cubic $\boldsymbol{x}$-, $\boldsymbol{y}$-, and $\boldsymbol{z}$-axes point along the three NN Ir–O bonds in an octahedron [see Fig. 1(a)] [14].

We first evidence that the directions of the orbital and spin moments of Na_2IrO_3 have a very slight deviation, strongly supporting the commonly accepted fact that the magnetism of Na_2IrO_3 is well described by the $J_{\text{eff}} = 1/2$ state [14,16,19,22]. Due to the trigonal distortion, the $J_{\text{eff}} = 1/2$ state of Na_2IrO_3 is not pure and mixed with the $J_{\text{eff}} = 3/2$ state. In this case, orbital and spin moments are not necessarily in exactly the same direction and deviate from each other. Hence, the optimal relative angle between orbital and spin moments itself is of fundamental importance. To figure out this optimal relative angle, we fix the orbital moments along four representative and important axes, namely, x-, y-, z-, and [110] axes, and we rotate the spin moments slightly away from the fixed orbital moments (for more details, see Appendix A). As shown in Figs. 1(c)–1(f), the optimal relative angles giving rise to the minima of the energy ΔE caused by the derivation between orbital and spin moments are fairly small and on the order of several degrees. More explicitly, they are 9°,

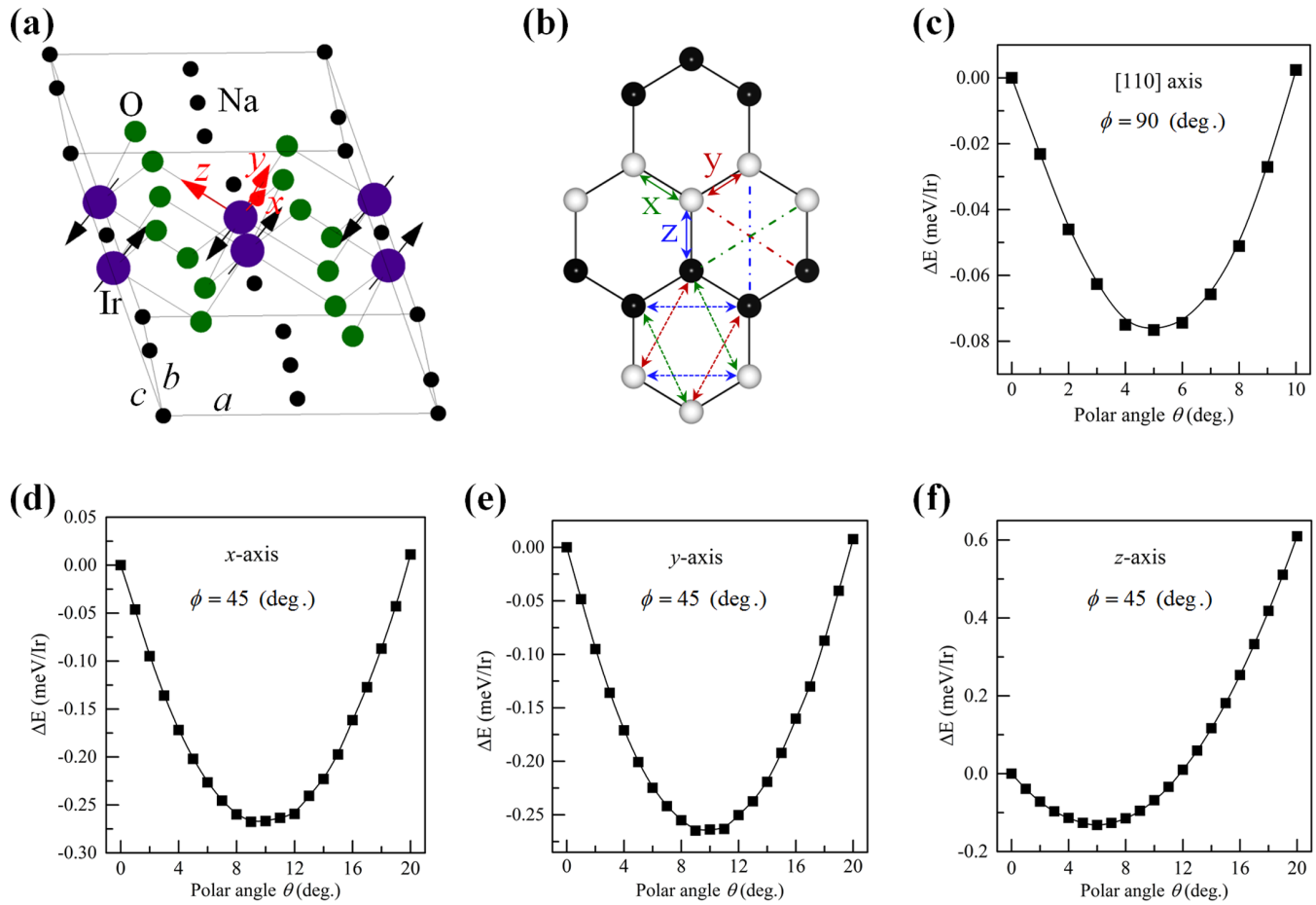

FIG. 1. (a) Crystal structure of the honeycomb Na_2IrO_3. Na, Ir, and O atoms are represented by the small black, large purple, and dark green medium-sized spheres, respectively. The cubic $\boldsymbol{x}$-, $\boldsymbol{y}$-, and $\boldsymbol{z}$-axes are the same as those used in Ref. [14] and are shown by the red arrows. The zigzag AFM order with magnetic moments along the [110] direction is shown by the black arrows. (b) The NN, second-NN, and third-NN Ir-Ir paths in the Ir atoms sublattice are connected by the solid double-arrowed, dashed double-arrowed, and dashed-dotted lines, respectively. The x-, y-, and z-bond Ir-Ir paths are distinguished by green, red, and blue. Black and white spheres have up and down spins, respectively. Dependences of the energy ΔE are caused by the derivation between the orbital and the spin moments on the polar angle θ of spin moment when the orbital moment is along the (c) [110], (d) x, (e) y, and (f) z axes.

9°, 6°, and 5°, respectively, when orbital moments are along the x-, y-, z-, and [110] axes. Therefore, it is reasonable to conclude that orbital and spin moments point along the same direction in Na_2IrO_3, as required by the $J_{\text{eff}} = 1/2$ state [26]. This is consistent with a recent theoretical study that asserts that Na_2IrO_3 is located in the relativistic $J_{\text{eff}} = 1/2$ Mott insulating region [37]. Therefore, the directions of orbital and spin moments are constrained to be exactly the same in our calculations hereafter.

To examine the magnetic ground state of Na_2IrO_3 theoretically, we consider eight different important magnetic orders. Four representative magnetic orders [Fig. 2(a)], namely the FM, Neél AFM, stripe AFM, and zigzag AFM orders, have been widely considered in previous studies [9,24,27]. Additionally, four more magnetic orders are also taken into consideration [Fig. 2(a)]. The first one is armchair AF order, in which the FM chain is propagating along the armchair edge in the honeycomb lattice. The other three magnetic orders are the zigzag-2 AFM, stripe-2 AFM, and armchair-2 AFM orders. These three magnetic orders are symmetrically nonequal to the above-mentioned zigzag AFM, stripe AFM, and armchair AFM orders because Na_2IrO_3 has the C_{2h} point space group rather than the C_{3v} point space group. Note that the zigzag-2 AFM structure is the same as the reported zigzag (X) order in a recent study of Na_2IrO_3 [38]. To determine the magnetic ground state, we considered nine different directions along which the magnetic moments align, namely $\boldsymbol{a}$, $\boldsymbol{b}$, $\boldsymbol{c}$, [100], [010], [001], [110], [101], and [011], for each magnetic order. Figure 2(b) shows the energy differences of the above-mentioned eight magnetic orders with respect to the zigzag-[110] order. As can be seen, the zigzag-[110] order has the lowest energy among them, as expected. Interestingly, the zigzag-2-[101] order has a comparable total energy with the ground-state zigzag-[110] order. To precisely determine the magnetic easy axis of the zigzag AFM order, we performed detailed investigations on its anisotropic energy. Here, the direction of magnetic moments is distinguished by the polar angle θ and azimuthal angle ϕ in the ($\boldsymbol{x}$, $\boldsymbol{y}$, $\boldsymbol{z}$) coordinate system, as shown in Fig. 1(a). By scanning θ and ϕ, we find that $\theta = 80^\circ$ and $\phi = 225^\circ$ have the lowest energy [Fig. 2(c)], that is to say, magnetic moments are parallel or antiparallel to the [441] direction. Actually, this direction

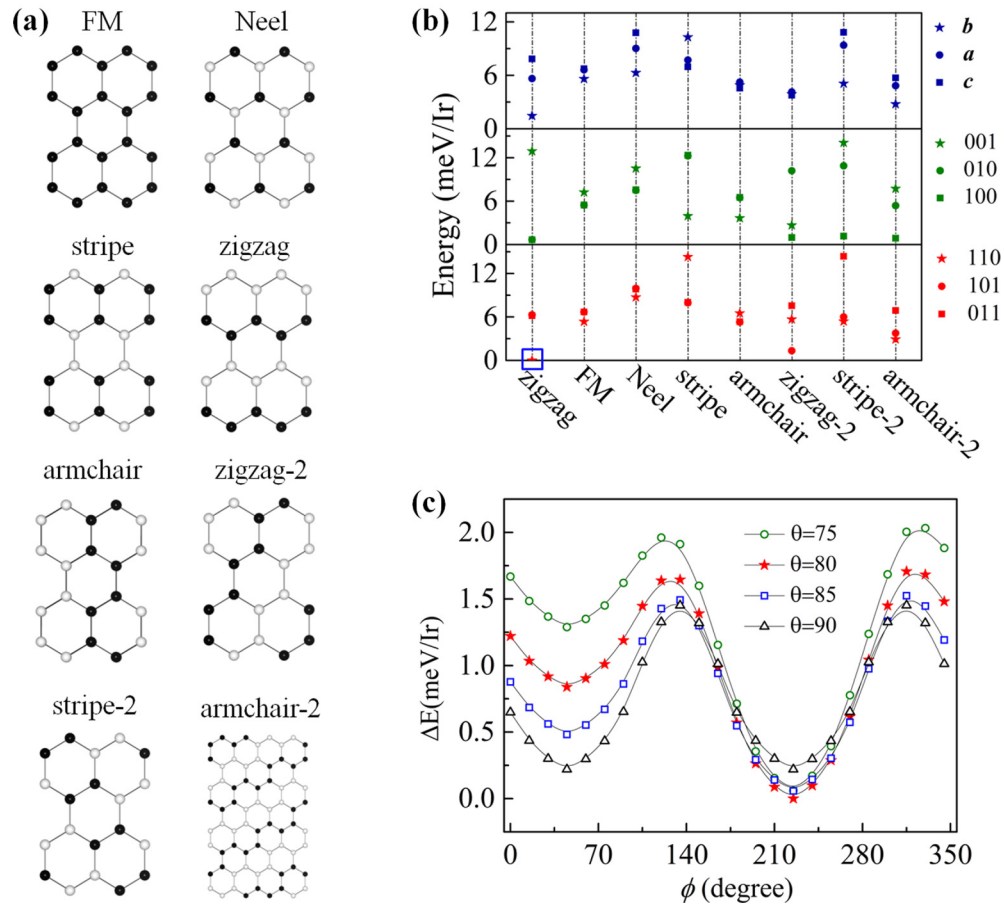

FIG. 2. (a) FM, Neél AFM, stripe AFM, zigzag AFM, armchair AFM, zigzag-2 AFM, stripe-2 AFM, and armchair-2 AFM magnetic orders. Black and white spheres have up and down spins, respectively. (b) The relative energies of the considered magnetic orders with magnetic moments along various directions. The zigzag AFM order with magnetic moments along the [110] direction (zigzag-[110]) has the lowest energy and is set as the energy reference, which is highlighted by the blue rectangle. (c) Energy dependence of the zigzag AFM order on the polar angle θ and azimuthal angle ϕ in the $(\boldsymbol{x}, \boldsymbol{y}, \boldsymbol{z})$-coordinate system [see Fig. 1(a)]. The energy of the case ($\theta = 80^\circ$, $\phi = 225^\circ$) is set as the energy reference. Because the cases of azimuthal θ ranging from 0° to 60° have relatively high energy, they are not shown here.

deviates slightly from the $\boldsymbol{x}y$-plane and approximately points along the [110] direction. The obtained magnetic easy axis, therefore, is consistent with the experimentally observed one [14]. Note that the conventional DFT calculations cannot find the zigzag AFM in another $J_{\text{eff}} = 1/2$ magnet α-$RuCl_3$ [27], while it found the zigzag AFM with the moments aligned along the local 110 direction in Na_2IrO_3 [24], indicating that our method of constraining the direction of orbital moments generally works well for the $J_{\text{eff}} = 1/2$ magnets.

B. Magnetic interaction parameters of Na_2IrO_3

To explore the nature of the zigzag antiferromagnetism of Na_2IrO_3, we consider the general bilinear exchange Hamiltonian, which has been widely adopted in previous studies of $J_{\text{eff}} = 1/2$ magnets [17,19,20,23,24,39] and has the form

$$H = \sum_{ij\in\alpha\beta(\gamma)} \big[J_{ij}\boldsymbol{S}_i\cdot\boldsymbol{S}_j + K_{ij}S_i^\gamma S_j^\gamma + \boldsymbol{D}_{ij} \cdot(\boldsymbol{S}_i\times\boldsymbol{S}_j) + \boldsymbol{S}_i\cdot\boldsymbol{\Gamma}_{ij}\cdot\boldsymbol{S}_j\big]. \quad (1)$$

In Eq. (1), i and j label Ir sites, and the pseudospin operator $\boldsymbol{S}_i$ is a $J_{\text{eff}} = 1/2$ state localized pseudospin operator with components S_i^α ($\alpha = \boldsymbol{x}, \boldsymbol{y}, \boldsymbol{z}$). Parameters J_{ij}, K_{ij}, and $D_{ij} = (D_{ij}^x, D_{ij}^y, D_{ij}^z)$ are the isotropic Heisenberg interaction, bond-dependent Kitaev interaction, and Dzyaloshinskii-Moriya (DM) vector, respectively. The last term is the generalized symmetric off-diagonal exchange [17], which is

$$\boldsymbol{S}_i\cdot\boldsymbol{\Gamma}_{ij}\cdot\boldsymbol{S}_j = \Gamma_{ij}^x\big(S_i^yS_j^z + S_i^zS_j^y\big) + \Gamma_{ij}^y\big(S_i^zS_j^x + S_i^xS_j^z\big) + \Gamma_{ij}^z\big(S_i^xS_j^y + S_i^yS_j^x\big). \quad (1a)$$

In this model, we consider the magnetic interactions up to the third-NN Ir-Ir pairs. Every Ir-Ir bond is labeled by one pseudospin direction $\gamma = (x, y, z)$ [see Fig. 1(b)] and two other directions α and β [17]. For convenience, hereafter the magnitude of the $J_{\text{eff}} = 1/2$ state localized magnetic moment is absorbed into the magnetic interaction parameters J_{ij}, K_{ij}, $\boldsymbol{D}_{ij}$, and $\boldsymbol{\Gamma}_{ij}$ so that the $J_{\text{eff}} = 1/2$ state localized pseudospins $\boldsymbol{S}_i$ and $\boldsymbol{S}_j$ are unit vectors.

Our calculated magnetic interaction parameters are listed in Table I. These magnetic interaction parameters are calculated

TABLE I. DFT calculated magnetic interaction parameters in units of meV of the general bilinear exchange Hamiltonian, Eq. (1). NNN and NNNN denote the second NN and the third NN, respectively. The bond distances of the Ir-Ir pairs are evaluated based on the experimentally measured crystal structure [11]. The last row shows the magnetic interaction parameters present in the minimal J_1-K_1-Γ_1-J_3 model.

J Path		d (Å)	J	K	Γ^x	Γ^y	Γ^z	D^x	D^y	D^z
NN	x/y	3.129	1.37	−9.56	−1.07	1.00	−1.22	0	0	0
	z	3.138	2.16	−11.00	−0.80	−0.89	0.66	0	0	0
NNN	x/y	5.425	0.08	−0.14	0.01	0.06	0.07	−0.12	−0.13	0.00
	z	5.427	0.16	−0.16	0.06	0.06	0.15	0.15	0.05	0.17
NNNN	z	6.257	0.82	0.14	−0.01	0.01	0.04	0.00	0.01	−0.03
	x/y	6.269	0.83	0.13	0.05	0.01	−0.02	0.01	−0.01	−0.01
Minimal model			J_1 1.63	K_1 −10.00		Γ_1 0.90			J_3 0.83	

by means of the variant from our previous four-state method [40], and its details are given in Appendix B. We see that the NN magnetic interactions are dominant. The NN Kitaev interactions are FM, consistent with the previous *ab initio* study result [22], and they dominate over other kinds of magnetic interactions by almost one order in magnitude. Although the NN x-/y-bonds and the NN z-bond have similarly strong FM Kitaev interactions, their AFM Heisenberg interactions are somewhat different. Our calculations indicate that the symmetric off-diagonal exchanges of the NN x-, y-, and z-bonds have three sizable components. One of them is AFM while the other two are FM. This is different from the originally proposed one-component symmetric off-diagonal exchange in Ref. [17]. Note that it is assumed in Ref. [17] that the Ir_2O_{10} cluster of Na_2IrO_3 has D_{2h} point symmetry, so that the symmetric off-diagonal exchange has only one component. The IrO_6 octahedrons in that cluster actually have tilts and rotations, however. Therefore, the Ir_2O_{10} cluster has C_{2h} point symmetry, and DFT calculated symmetric off-diagonal exchanges have three components, which is indeed in agreement with the case discussed in the supplementary material of Ref. [17]. In addition to the above findings, we also find that the third-NN Heisenberg interactions are unexpectedly sizable while the second-NN magnetic interactions are extremely weak compared with the NN ones. It is surprising that the third-NN AFM Heisenberg interactions are even comparable to the NN ones since the bond distances of the third-NN Ir-Ir pairs are about twice as long as those of the NN Ir-Ir pairs (see Table I). The underlying physical reasons for such results will be discussed later. Lastly, the NN Ir-Ir pairs have exactly vanishing DM interactions as they have inversion symmetry. For second- and third-NN Ir-Ir pairs, their DM interactions are all extraordinarily weak. Considering those, DM interactions are not included further in the following discussions.

Using our calculated magnetic interaction parameters, we perform efficient exchange Monte Carlo (MC) [34–36] simulation and well reproduce that the magnetic ground state is the zigzag AFM order and its magnetic easy axis is almost along the [110] direction, which is consistent with experimental observations [14]. Moreover, our MC simulation shows that the magnetic transition temperature is about 18.9 K, quite close to the experimentally measured $T_N = 18.1$ K [10]. This result, therefore, further rationalizes our calculated magnetic interaction parameters using our newly proposed methods.

C. $J_{\text{eff}} = 1/2$ Wannier orbitals of Na_2IrO_3

To reveal why the long-range third-NN Heisenberg interactions are sizable but the second-NN magnetic interactions are so weak in Na_2IrO_3, we construct four $J_{\text{eff}} = 1/2$ Wannier orbitals in the primitive cell of Na_2IrO_3 [41]. In the cubic crystal field, $J_{\text{eff}} = 1/2$ states are in the form of [25]

$$|J_{\text{eff}} = 1/2, 1/2\rangle = \frac{1}{\sqrt{3}}|xy, \uparrow\rangle + \frac{i}{\sqrt{3}}|zx, \downarrow\rangle + \frac{1}{\sqrt{3}}|yz, \downarrow\rangle, \tag{2a}$$

$$|J_{\text{eff}} = 1/2, -1/2\rangle = \frac{1}{\sqrt{3}}|xy, \downarrow\rangle + \frac{i}{\sqrt{3}}|zx, \uparrow\rangle - \frac{1}{\sqrt{3}}|yz, \uparrow\rangle. \tag{2b}$$

According to Eq. (2a), the $|J_{\text{eff}} = 1/2, 1/2\rangle$ Wannier orbital consists of three components, namely a real part of spin-up, an imaginary part of spin-down, and a real part of spin-down. Similarly, the $|J_{\text{eff}} = 1/2, -1/2\rangle$ Wannier orbital [see Eq. (2b)] is composed of three components as well, namely a real part of spin-down, an imaginary part of spin-up, and a real part of spin-up. To construct the desired Wannier orbitals using MLWFs, we chose an energy window from −0.3 to 0.2 eV in which four isolated bands are included, as shown in the DFT+SOC calculated band structure [Fig. 3(a)]. The red dashed-dotted lines are the Wannier-interpolated four bands, which well reproduce the DFT calculated bands, indicating that $J_{\text{eff}} = 1/2$ Wannier orbitals are well constructed.

The $J_{\text{eff}} = 1/2$ Wannier orbitals distribute appreciably over the three NN Ir atoms. Figures 3(c)–3(e) show the spatial distribution of the three components of the $|J_{\text{eff}} = 1/2, 1/2\rangle$ Wannier orbital for the reference Ir-0 atom. As expected, the Wannier centers of the three components of this Wannier orbital are located near the reference Ir-0 site. In addition, appreciable tails show up distributing over the three NN Ir sites of the reference Ir-0 atom [labeled by Ir-1, Ir-2, and Ir-3 in Fig. 3(c)]. Consequently, for a specified third-NN Ir-Ir pair, their two $|J_{\text{eff}} = 1/2, 1/2\rangle$ Wannier orbitals are closely connected by their tails [see Fig. 3(b)]. Due to distortion of the IrO_6 octahedrons, the $|J_{\text{eff}} = 1/2, 1/2\rangle$ Wannier orbital is slightly contaminated by the extra imaginary part of the spin-up [Fig. 3(f)]. Likewise, The $|J_{\text{eff}} = 1/2, -1/2\rangle$ Wannier orbital is widely distributed over the three NN Ir atoms, but is slightly contaminated by the extra imaginary part of the spin-down. Note that such a spatial distribution of the $J_{\text{eff}} = 1/2$ Wannier

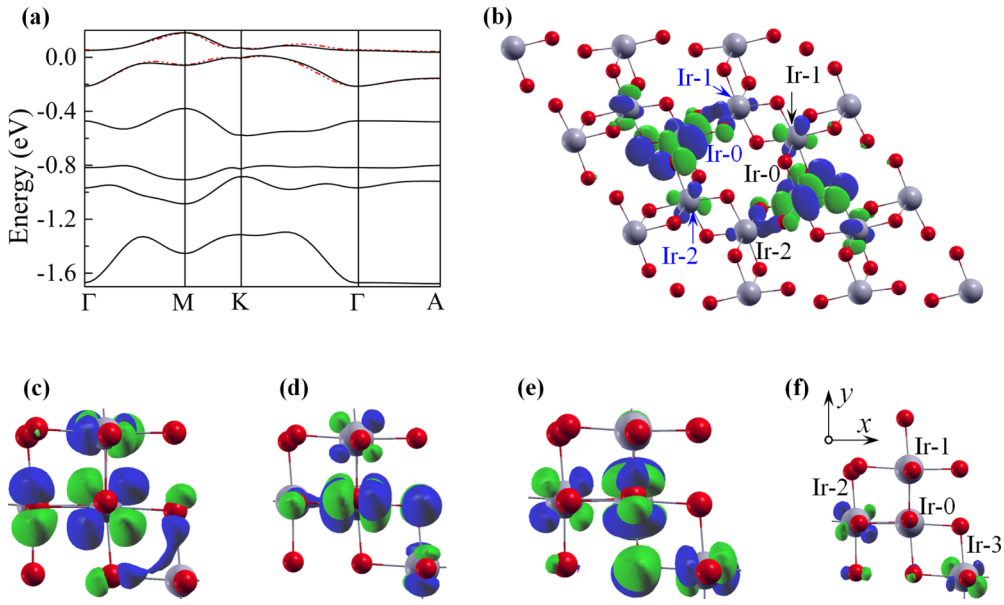

FIG. 3. (a) DFT+SOC calculated band structure (black line) of Na_2IrO_3 and Wannier-interpolated four bands (the red dashed-dotted lines) near the Fermi level ($E_{\text{Fermi}} = 0$). (b) Real parts of spin-up of the two $|J_{\text{eff}} = 1/2, 1/2\rangle$ Wannier orbitals of the third-NN Ir-Ir pair (black and blue labels "Ir-0") in the $3 \times 3 \times 1$ supercell of the Na_2IrO_3 primitive cell. (c) Real part of spin-up, (d) imaginary part of spin-down, (e) real part of spin-down, and (f) imaginary part of spin-up of the calculated $|J_{\text{eff}} = 1/2, 1/2\rangle$ Wannier orbital on the Ir-0 atom. The three NN Ir atoms of the Ir-0 atom are labeled by Ir-1, Ir-2, and Ir-3 as shown in (f). Wannier orbitals in (c)–(f) are viewed along the z axis, but they are viewed along the crystallographic c axis in (b). The maximum (minimum) grid values are 7.2 (−7.0) in (c)–(e) and 0.9 (−0.9) in (f). The isosurface value is 1.5 in (b)–(e) and 0.4 in (f).

orbitals is also reported in the previous study of the honeycomb α-Li_2IrO_3 [42].

In the $J_{\text{eff}} = 1/2$ Wannier orbital manifold, the model Hamiltonian is [42,43]

$$H_{\text{eff}} = \sum_{\langle i,j\rangle\sigma} t_{n1}^{\boldsymbol{r}_{ij}} c_{i,\sigma}^{\dagger} c_{j,\sigma} + \sum_{\langle\langle i,j\rangle\rangle\sigma\sigma'} t_{n2;\sigma\sigma'}^{\boldsymbol{r}_{ij}} c_{i,\sigma}^{\dagger} c_{j,\sigma'} + \sum_{\langle\langle\langle i,j\rangle\rangle\rangle\sigma\sigma'} t_{n3}^{\boldsymbol{r}_{ij}} c_{i,\sigma}^{\dagger} c_{j,\sigma}. \tag{3}$$

In Eq. (3), hopping parameters are represented in terms of Pauli matrices [43], such as

$$t_{\sigma\sigma'}^{\boldsymbol{r}_{ij}} = C_{\boldsymbol{r}_{ij}}^{0} \delta_{\sigma\sigma'} + \boldsymbol{C}_{\boldsymbol{r}_{ij}} \cdot \tau_{\sigma\sigma'}, \tag{4}$$

where $\boldsymbol{\tau}=(\boldsymbol{\sigma}_x, \boldsymbol{\sigma}_y, \boldsymbol{\sigma}_z)$ is the vector of the Pauli matrices, $\boldsymbol{C} = (C_x, C_y, C_z)$, $\boldsymbol{\sigma}$, $\boldsymbol{\sigma}' = \pm$ represent the $J_{\text{eff}} = 1/2$ Wannier orbitals, and the parameter $\boldsymbol{r}_{ij}$ is the displacement vector between two different Ir sites i and j. Considering the direct exchange process between two different Wannier orbitals of the $J_{\text{eff}} = 1/2$ state, magnetic interaction parameters can be estimated directly by [43]

$$J_{ij} = \frac{4}{U}\left(C_{ij}^{0} C_{ji}^{0} - \boldsymbol{C}_{ij} \cdot \boldsymbol{C}_{ji}\right), \tag{5a}$$

$$\boldsymbol{D}_{ij} = -\frac{4I}{U}\left(C_{ji}^{0} \boldsymbol{C}_{ij} - C_{ij}^{0} \boldsymbol{C}_{ji}\right), \tag{5b}$$

$$\boldsymbol{\Gamma}_{ij} = \frac{4}{U}\left(\boldsymbol{C}_{ij}\boldsymbol{C}_{ji} + \boldsymbol{C}_{ji}\boldsymbol{C}_{ij}\right). \tag{5c}$$

In Eq. (5b), the italic letter I is the imaginary unit.

Surprisingly, the third-NN hopping is stronger than that of the NN and second NN. It is shown in Table II that the third-NN hopping parameters are about three times as large as those of the second NN. Because the direct exchange process dominantly contributes to the magnetic interactions of the second- and third-NN Ir-Ir pairs, we can estimate, based on Eq. (5a), that the Heisenberg interaction of the third-NN Ir-Ir pairs should be stronger by approximately one order of magnitude compared to those of the second-NN Ir-Ir pairs. Such an estimation agrees with the DFT calculated NN and third-NN Heisenberg interaction parameters (see Table I). In addition, the second-NN Ir-Ir pairs have similarly small parameters $C_{r_{ij}}^{0}$ and $C_{r_{ij}}$, so their symmetric off-diagonal exchanges and DM interactions are weak, which is also consistent with our DFT calculated results. Note that the NN Ir-Ir pairs have strong magnetic interactions, although they have small hopping parameters in the $J_{\text{eff}} = 1/2$ Wannier orbital manifold.

TABLE II. Hopping parameters in units of meV of the NN, second-NN (NNN), and third-NN (NNNN) Ir-Ir paths in terms of the $J_{\text{eff}} = 1/2$ Wannier orbital representation.

Ir-Ir bond		$C_{r_{ij}}^{0}$	$-iC_{r_{ij}}^{x}$	$-iC_{r_{ij}}^{y}$	$-iC_{r_{ij}}^{z}$
NN	x	−0.9			
	y	−0.8			
	z	9.8			
NNN	x	−5.8	11.4	6.3	−5.3
	y	−5.8	−11.1	5.8	6.31
	z	−7.3	3.7	−11.2	11.6
NNNN	x	−39.0			
	y	−38.8			
	z	−38.3			

The smaller NN hopping than the NNNN hopping is due to the cancellation between different hopping contributions, including d-d and d-p-d hopping processes [42]. Since the NN Heisenberg interactions have rather different dependences on their various hopping processes [21,43], we cannot estimate them based on the hopping parameters between the $J_{\rm eff} = 1/2$ Wannier orbitals.

Sizable long-range third-NN AFM Heisenberg interactions closely correlate with the appreciable distribution of Wannier orbitals of $J_{\rm eff} = 1/2$ states over the three NN Ir atoms. We have shown that the third-NN Ir-Ir pair has two closely connected $J_{\rm eff} = 1/2$ Wannier orbitals due to the appreciable tails of $J_{\rm eff} = 1/2$ Wannier orbitals distributing over the three NN Ir atoms. Therefore, it is acceptable that the third-NN Ir-Ir pair has a sizable magnetic interaction. If the tails of these two $J_{\rm eff} = 1/2$ Wannier orbitals were removed, they would be far away from each other. In that case, the third-NN Ir-Ir pair should have a weak magnetic interaction. To verify this, we artificially removed the tails of the two $J_{\rm eff} = 1/2$ Wannier orbitals of the third-NN Ir-Ir pair [see Fig. 3(b)] by replacing the four bridging Ir atoms [the Ir atoms labeled by the black and blue Ir-1 and Ir-2 in Fig. 3(b)] with isovalent Si and Ti atoms. Our DFT calculations show that the third-NN Heisenberg interaction significantly reduces to −0.11 meV in the case of Si and to 0.04 meV in the case of Ti from the original 0.82 meV. Such a significant reduction indicates that the tails of the $J_{\rm eff} = 1/2$ Wannier orbital are indeed critical to give rise to the sizable long-range third-NN Heisenberg interaction.

D. Minimal J_1-K_1-Γ_1-J_3 model of Na_2IrO_3

The general bilinear exchange model, Eq. (1), has many magnetic interaction parameters, which masks the underlying physics of the zigzag antiferromagnetism of Na_2IrO_3. Actually, some of them are negligible and can be reasonably ignored, and some can be reasonably merged, too. Consequently, a simplified and concise model can be achieved by considering the dominant magnetic interactions. To do this, we put forward a minimal J_1-K_1-Γ_1-J_3 model based on our understanding and the calculated magnetic interaction parameters. Our minimal model is in the form of

$$H = \sum_{\langle ij\rangle\in\alpha\beta(\gamma)} \big[J_1 \boldsymbol{S}_i\cdot\boldsymbol{S}_j + K_1 S_i^\gamma S_j^\gamma + \Gamma_1\big(S_i^\alpha S_j^\beta + S_i^\beta S_j^\alpha - S_i^\alpha S_j^\gamma - S_i^\gamma S_j^\alpha - S_i^\gamma S_j^\beta - S_i^\beta S_j^\gamma\big)\big] + \sum_{\langle\langle\langle ij\rangle\rangle\rangle\in\alpha\beta(\gamma)} J_3 \boldsymbol{S}_i\cdot\boldsymbol{S}_j. \quad (6)$$

In this model, the second-NN magnetic interactions are not taken into consideration since they are much weaker than the NN and the third-NN ones. It is worthwhile noting that the off-diagonal symmetric exchange Γ_1 in our model has three components, which is significantly different from the previous theoretical models. Although the NN (the third-NN) x-/y-bonds and z-bond are symmetrically nonequivalent, they are considered to be symmetrically equivalent for simplicity. As for the third-NN x-, y-, and z-bond Ir-Ir pairs, only their Heisenberg interactions are involved in this model. The magnitudes of the magnetic interaction parameters J_1, K_1, Γ_1, and J_3 in this minimal model are obtained by averaging the corresponding DFT calculated ones, which are listed in Table I. Our MC simulations of the minimal J_1-K_1-Γ_1-J_3 model with those parameters show that its magnetic ground state is the zigzag AFM with the magnetic easy axis along the [110] direction, and its magnetic transition temperature is 17.4 K, very close to the experimentally observed $T_{\rm N} = 18.1$ K [10]. Thus, this model describes the experimentally observed zigzag antiferromagnetism of Na_2IrO_3 well.

The magnetic excitations of the minimal J_1-K_1-Γ_1-J_3 model have an intensity peak at 5.6 meV, highly consistent with the inelastic neutron-scattering experiment [11]. Because of the breakdown of magnons in the strongly spin-orbital-coupled magnet [44,45], we studied the magnons of Na_2IrO_3 by numerically calculating dynamical structure factors based on the exact diagonalization (ED) computations. Here the dynamical structure factor at zero temperature is defined as [46]

$$I^{\alpha\beta}(\boldsymbol{Q},\omega) = -\frac{1}{\pi}\mathrm{Im}\left[\langle 0|O^{\alpha\dagger}\frac{1}{\omega + E_0 + i\varepsilon - H}O^{\beta}|0\rangle\right]. \quad (7)$$

In Eq. (7), $|0\rangle$ is the ground-state wave function of H with the energy E_0 and the operator $O^\alpha = N^{-1}\sum_{\boldsymbol{r}} S^\alpha \exp(-i\,\boldsymbol{Q}\cdot\boldsymbol{r})$. The ground-state wave function $|0\rangle$ and energy E_0 are calculated by the Lanczos method [46], and the intensity $I(\boldsymbol{Q},\omega) = \sum_{\alpha=x,y,z} I^{\alpha\alpha}(\boldsymbol{Q},\omega)$ is obtained by a continued fraction expansion [45–47]. Similar to previous studies [44,45], we take into account two different 24-site periodic clusters compatible with the zigzag AFM order, namely the UC-3×2 [Fig. 4(a)] and $\sqrt{3}\times\sqrt{3}$ -2×2 [Fig. 4(b)] clusters. The energy scan of the dynamical structure factor [Fig. 4(c)] shows that the magnetic excitations of the UC-3×2 cluster has an intensity peak at 5.6 meV, consistent with the experimentally measured spin-wave intensity peak at 5.0 meV in the inelastic neutron-scattering experiment [11]. Actually, the magnetic excitation of the $\sqrt{3}\times\sqrt{3}$ -2×2 cluster has an intensity peak at 2.6 meV [Fig. 4(c)], which should be in accordance with the potential spin-wave intensity peak near 2.0 meV in the inelastic neutron-scattering experiment [11]. Note that the latter intensity peak is not well-defined in the inelastic neutron-scattering experiment because of the limitation of the instrumental energy resolution [11]. Therefore, our theoretical result calls for further experimental magnon measurement to clearly identify the possible *hidden* intensity peak so as to comprehensively unveil the nature of the zigzag antiferromagnetism in Na_2IrO_3.

The experimentally observed zigzag AFM structure is cooperatively established by the NN symmetric off-diagonal exchange and the third-NN AFM Heisenberg interaction. If only the NN FM Kitaev interaction K_1 and the NN AFM Heisenberg interactions J_1 are considered, MC simulations show that the magnetic ground state is the stripe AFM, the same as the previous study result [21]. To unravel why Na_2IrO_3 has [110]-oriented zigzag AFM order, we determined the preferred magnetic orders in the Γ_1-J_3 plane by fixing the NN Heisenberg interaction J_1 and the Kitaev interaction K_1. To this end, we use the classical Luttinger-Tisza (LT) method in which the pseudospins are considered to be classical moments, and the constant length pseudospin vectors are replaced by the unconstrained vector fields $\vec{\phi}_{\boldsymbol{r}}$. In this case, the classical Hamiltonian written in the momentum space of the unit cell

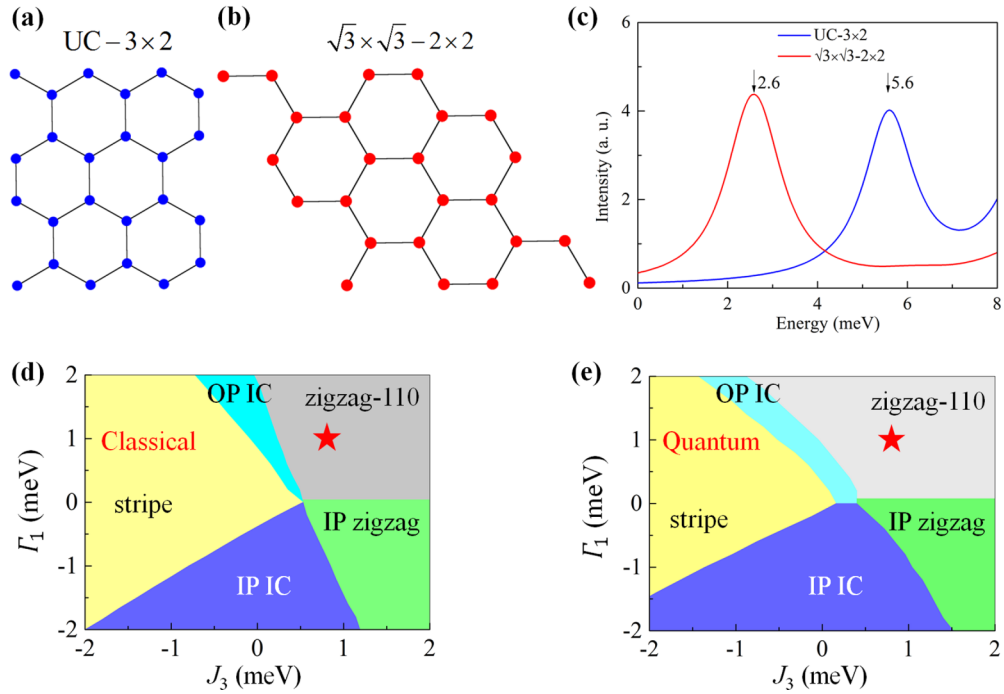

FIG. 4. (a) 24-site periodic $UC-3\times2$ and (b) $\sqrt{3}\times\sqrt{3}-2\times2$ clusters. (c) ED calculated energy-dependent magnetic excitation intensity of the minimal J_1-K_1-Γ_1-J_3 model whose magnetic parameters are listed in Table I. A Gaussian broadening of 0.67 meV (FWHM), same as the instrumental energy resolution in Ref. [11], has been adopted. The intensity peaks of the $UC-3\times2$ (blue) and $\sqrt{3}\times\sqrt{3}-2\times2$ (red) clusters are indicated by the black arrows. Classical (d) and quantum (e) phase diagrams of the minimal J_1-K_1-Γ_1-J_3 model in the Γ_1-J_3 plane. The NN Heisenberg J_1 and Kitaev interactions K_1 are 1.63 and -10.0 meV, respectively. The red stars highlight the specific position ($J_3=0.83$ meV, $\Gamma_1=0.90$ meV) in the Γ_1-J_3 plane. The out-of-plane (OP) incommensurate (IC) and the in-plane (IP) IC phase regions can be much richer than the standard coplanar helix states.

(containing four Ir atoms) of Na_2IrO_3 is

$$H_{LT}(\boldsymbol{k})=\sum_{\boldsymbol{k}}\phi^{\dagger}_{\boldsymbol{k}\mu}\Lambda_{\mu\nu}(\boldsymbol{k})\phi_{\boldsymbol{k}\nu}. \tag{8}$$

In Eq. (8), the Hamiltonian $\Lambda(\boldsymbol{k})$ is a 12-by-12 matrix that is dependent on the magnetic interactions parameters J_1, K_1, Γ_1, and J_3 (see the details in Appendix C). Figure 4(d) shows the phase diagram obtained by numerically minimizing the Hamiltonian $\Lambda(\boldsymbol{k})$ in the first Brillouin zone. It is shown by Fig. 4(d) that the third-NN AFM Heisenberg interaction J_3 stabilizes the zigzag AFM order. This is reasonable, because the third-NN AFM Heisenberg interaction is magnetically satisfied in the zigzag AFM order [see Fig. 1(b)]. In addition, the NN symmetric off-diagonal exchange can determine the magnetic easy axis of the zigzag AFM order: (i) if it is FM, magnetic moments will lie in the $\boldsymbol{ab}$ plane; (ii) if it is AFM, the magnetic moments will be along the [110] direction, namely the experimentally observed one. Hence it is the cooperation between the NN symmetric off-diagonal exchange Γ_1 and the third-NN AFM Heisenberg interaction J_3 that establishes the experimentally observed zigzag AFM structure.

Quantum fluctuations have almost no significant effect on the preferred magnetic orders obtained by the LT method, except for the phase boundary. Because the $J_{\rm eff}=1/2$ state is an analog to the $S=1/2$ state [6], it would have strong quantum fluctuations. To elucidate the effect of quantum fluctuations, we additionally carried out an ED computation on the 24-site UC-3×2 cluster [Fig. 4(a)]. We calculated the static spin-structure factor

$$S(\boldsymbol{Q})=\sum_{ij}\langle\boldsymbol{S}_i\cdot\boldsymbol{S}_j\rangle\exp[i\,\boldsymbol{Q}\cdot(\boldsymbol{r}_i-\boldsymbol{r}_j). \tag{9}$$

The dominant magnetic order is determined according to the wave number $\boldsymbol{Q}=\boldsymbol{Q}_{\rm max}$, which has a maximum in the static spin-structure factor $S(\boldsymbol{Q})$. Figure 4(e) shows the phase diagram obtained in the ED study. By comparing the phase diagram obtained by the LT method with that obtained by the ED computation, one can see that all of the classical magnetic orders obtained by the LT method are recovered by the ED computation except that their phase boundary positions are different. Most importantly, the ED computation also shows that the NN symmetric off-diagonal exchange and the third-NN Heisenberg interaction cooperatively establish the experimentally observed zigzag AFM structure.

IV. DISCUSSION AND SUMMARY

It is possible that honeycomb $J_{\rm eff}=1/2$ magnets generally have a sizable long-range third-NN Heisenberg interaction. Here we underline that the sizable long-range third-NN Heisenberg interaction in Na_2IrO_3 is robust and independent of the choice of the on-site Coulomb energy U (see Appendix D), similar to our previous results in the honeycomb $J_{\rm eff}=1/2$ magnet α-$RuCl_3$ [27]. It has been reported that the honeycomb α-Li_2IrO_3 also has relatively strong third-NN hopping parameters [42], and its third-NN Heisenberg interaction is

even stronger than the first-NN Heisenberg interaction [20]. We note that there are Ir-Ir pairs with bond distances of about 6.0 Å, which is close to the bond distance of the third-NN Ir-Ir pairs in the honeycomb Na_2IrO_3, in the three-dimensional hyper-honeycomb β-Li_2IrO_3 [48], and the stripe-honeycomb γ-Li_2IrO_3 [49]. Therefore, these two three-dimensional iridates are new platforms to investigate whether the long-range third NN Heisenberg interaction is sizable, and they deserve further study.

In summary, we have fully studied the magnetic interactions of the honeycomb Na_2IrO_3 via our newly developed method and the maximally localized Wannier functions. We find that the long-range third-NN Ir-Ir pairs have sizable AFM Heisenberg interactions. We demonstrate that the sizable long-range third-NN AFM Heisenberg interaction closely correlates with the appreciable distribution of Wannier orbitals of $J_{\text{eff}} = 1/2$ states over the three NN Ir atoms. We propose a minimal J_1-K_1-Γ_1-J_3 model for Na_2IrO_3 and further show that its magnetic excitations have an intensity peak at 5.6 meV, highly consistent with the inelastic neutron-scattering experiment [11]. Our work shows that our newly developed method is a powerful way to study the magnetism of materials with non-negligible orbital moments, such as $J_{\text{eff}} = 1/2$ magnets, and it is a significant step toward understanding the novel magnetism of honeycomb $J_{\text{eff}} = 1/2$ magnets.

ACKNOWLEDGMENTS

This paper was partially supported by the National Natural Science Foundation of China and the Research Program of Shanghai Municipality, the Ministry of Education, and Fok Ying Tung Education Foundation.

APPENDIX A: THE OPTIMAL RELATIVE ANGLE BETWEEN ORBITAL AND SPIN MOMENTS

To evaluate the optimal relative angle between orbital and spin moments in Na_2IrO_3, we fix orbital moments along four representative and important axes, namely, x-, y-, z-, and [110] axes, and we rotate spin moments slightly away from the fixed orbital moments. We define the derivation between orbital and spin moments by a spherical coordinate system in which the polar angle θ is inclined from the fixed orbital moments, and the azimuthal angle ϕ lies on the plane perpendicular to the fixed orbital moments. In such a definition, the relative angle between orbital and spin moments is the polar angle θ. Note that any angle θ has an extra degree of freedom, namely the azimuthal angle ϕ. To obtain the correct energy ΔE caused by the derivation between orbital and spin moments with a given θ and ϕ, we should calculate the energies of two different cases. For the first case with the energy $E_1(\theta, \phi)$, the orbital moment is fixed at a given axis, for example the z axis, and the spin moment is along the direction with the polar angle θ and the azimuthal angle ϕ. For the second case with the energy $E_2(\theta, \phi)$, the orbital and spin moments are both in the same direction, which is along the vector sum of the orbital and spin moments of the first case. Because the general bilinear exchange Hamiltonian Eq. (1) in the main text is anisotropic due to its anisotropic exchange interactions, the second case

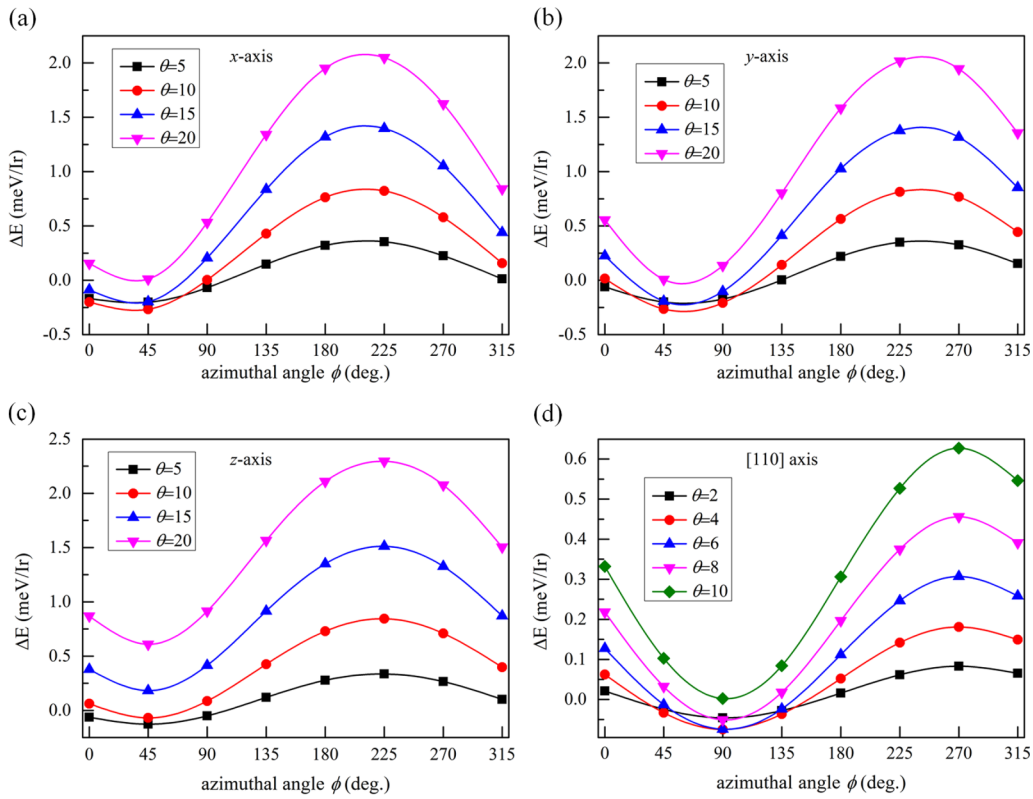

FIG. 5. Dependences of the energy ΔE on the polar angle θ and the azimuthal angle ϕ of the spin moment when the orbital moment is along the (a) x, (b) y, (c) z, and (d) [110] axes.

is actually a reference of the first case. Altogether, the energy ΔE is calculated by $\Delta E = E_1(\theta, \phi) - E_2(\theta, \phi)$.

The dependences of the energy ΔE on the polar angle θ and the azimuthal angle ϕ of spin moment (Fig. 5) indicate that the optimal relative angle between orbital and spin moments should be found with the azimuthal angle ϕ equal to 45° when the orbital moment is along the x-, y-, and z-axis. However, when the orbital moment is along the [110] axis, the optimal relative angle should be found with the azimuthal angle ϕ equal to 90°. In the main text, we explore in detailed the dependences of the energy ΔE with the specified azimuthal angles ϕ according to the above-mentioned facts. We find that the optimal relative angles between orbital and spin moments are 9°, 9°, 6°, and 5°, respectively, when the orbital moments are along the x-, y-, z-, and [110] axes. In principle, the orbital moment should scan all the directions to assess the optimal relative angle. Obviously, that is intractable practically. In any case, we argue based on the four representative and important directions of orbital moments that the optimal relative angle between the orbital and spin moment is rather small and in the order of several degrees.

APPENDIX B: VARIANT OF THE FOUR-STATE METHOD FOR CALCULATING MAGNETIC INTERACTIONS IN THE HAMILTONIAN EQ. (1)

Here are the details of the variant from our previous four-state method [40] to calculate the magnetic interaction parameters in the general bilinear exchange Hamiltonian Eq. (1) in the main text. Another form of the Hamiltonian Eq. (1) is as follows:

$$H = \sum_{ij} \sum_{\alpha\beta} J_{ij}^{\alpha\beta} S_i^{\alpha} S_j^{\beta}. \tag{B1}$$

In Eq. (B1), i and j are the indexes of magnetic sites, and α and β run over x, y, and z. Note that the $J_{ij}^{\alpha\beta}$ in the Hamiltonian Eq. (B1) is a 3-by-3 matrix for a specific ij bond, and the exchange parameters in the Hamiltonian Eq. (1) are obtained by appropriate combinations of the elements of the matrix $J_{ij}^{\alpha\beta}$. We take the ij bond belonging to the $xy(z)$ type as an example. In this case, we have

$$J_{ij} = \left(J_{ij}^{xx} + J_{ij}^{yy}\right)/2, \tag{B2a}$$

$$K_{ij} = J_{ij}^{zz} - \left(J_{ij}^{xx} + J_{ij}^{yy}\right)/2, \tag{B2b}$$

$$\Gamma_{ij}^{\alpha} = \left(J_{ij}^{\beta\gamma} + J_{ij}^{\gamma\beta}\right)/2, \tag{B2c}$$

$$D_{ij}^{\alpha} = \left(J_{ij}^{\beta\gamma} - J_{ij}^{\gamma\beta}\right)/2. \tag{B2d}$$

For the $J_{\text{eff}} = 1/2$ magnets, J_{ij}^{xx} is equal to J_{ij}^{yy} theoretically in Eq. (B2a). Now we show how to calculate any element of the matrix $J_{ij}^{\alpha\beta}$ for a specific ij bond. To this end, we rearrange the items in the Hamiltonian Eq. (B1) as follows:

$$H = \sum_{\alpha\beta} J_{ij}^{\alpha\beta} S_i^{\alpha} S_j^{\beta} + \sum_{k\neq i,j} \sum_{\alpha\beta} J_{ik}^{\alpha\beta} S_i^{\alpha} S_k^{\beta} + \sum_{k\neq i,j} \sum_{\alpha\beta} J_{kj}^{\alpha\beta} S_k^{\alpha} S_j^{\beta} + \sum_{k\neq i,j;m\neq i,j} \sum_{\alpha\beta} J_{km}^{\alpha\beta} S_k^{\alpha} S_m^{\beta}. \tag{B3}$$

As a concrete example, we consider the element J_{ij}^{xy}. To calculate this element, we set four different magnetic configurations (we denote the magnetic direction of any magnetic site as $[S_x, S_y, S_z]$), and we obtain their corresponding energy to the Hamiltonian Eq. (B3) as follows:

(i) The magnetic directions of sites i and j are [1,0,0] and [0,1,0], respectively, and the energy is

$$E_1 = J_{ij}^{xy} + \sum_{k\neq i,j} \sum_{\alpha} J_{ik}^{x\beta} S_k^{\beta} + \sum_{k\neq i,j} \sum_{\alpha} J_{kj}^{\alpha y} S_k^{\alpha} + \sum_{k\neq i,j;m\neq i,j} \sum_{\alpha\beta} J_{km}^{\alpha\beta} S_k^{\alpha} S_m^{\beta}. \tag{B3a}$$

(ii) The magnetic directions of sites i and j are [1,0,0] and [0,−1,0], respectively, and the energy is

$$E_2 = -J_{ij}^{xy} + \sum_{k\neq i,j} \sum_{\beta} J_{ik}^{x\beta} S_k^{\beta} - \sum_{k\neq i,j} \sum_{\alpha} J_{kj}^{\alpha y} S_k^{\alpha} + \sum_{k\neq i,j;m\neq i,j} \sum_{\alpha\beta} J_{km}^{\alpha\beta} S_k^{\alpha} S_m^{\beta}. \tag{B3b}$$

(iii) The magnetic directions of sites i and j are [−1,0,0] and [0,1,0], respectively, and the energy is

$$E_3 = -J_{ij}^{xy} - \sum_{k\neq i,j} \sum_{\beta} J_{ik}^{x\beta} S_k^{\beta} + \sum_{k\neq i,j} \sum_{\alpha} J_{kj}^{\alpha y} S_k^{\alpha} + \sum_{k\neq i,j;m\neq i,j} \sum_{\alpha\beta} J_{km}^{\alpha\beta} S_k^{\alpha} S_m^{\beta}. \tag{B3c}$$

(iv) The magnetic directions of sites i and j are [−1,0,0] and [0,−1,0], respectively, and the energy is

$$E_4 = J_{ij}^{xy} - \sum_{k\neq i,j} \sum_{\beta} J_{ik}^{x\beta} S_k^{\beta} - \sum_{k\neq i,j} \sum_{\alpha} J_{kj}^{\alpha y} S_k^{\alpha} + \sum_{k\neq i,j;m\neq i,j} \sum_{\alpha\beta} J_{km}^{\alpha\beta} S_k^{\alpha} S_m^{\beta}. \tag{B3d}$$

Based on Eqs. (B3a)–(B3b), we can obtain the element J_{ij}^{xy} in the form of

$$J_{ij}^{xy} = (E_1\text{-}E_2\text{-}E_3 + E_4)/4. \tag{B4}$$

Note that Eq. (B4) has the same form as Eq. (3) in Ref. [40]. After we obtain the nine elements of the matrix $J_{ij}^{\alpha\beta}$, we can figure out based on Eqs. (B2a)–(B2d) the magnetic interaction parameters J_{ij}, K_{ij}, $\boldsymbol{D}_{ij}$, and $\boldsymbol{\Gamma}_{ij}$ as shown in the Eq. (1) in the main text.

APPENDIX C: THE CLASSICAL LUTTINGER-TISZA HAMILTONIAN IN MOMENTUM SPACE

In the momentum space of the unit cell of Na_2IrO_3, which contains four Ir atoms, the classical Hamiltonian $\Lambda(\boldsymbol{k})$ [see Eq. (8) in the main text] obtained by the classical Luttinger-Tisza approximation is a 12-by-12 matrix, which is of the form

$$\Lambda(\boldsymbol{k}) = \begin{bmatrix} 0 & H_{12} & 0 & H_{14} \\ H_{12}^{\dagger} & 0 & H_{23} & 0 \\ 0 & H_{23}^{\dagger} & 0 & H_{34} \\ H_{14}^{\dagger} & 0 & H_{34}^{\dagger} & 0 \end{bmatrix}. \tag{C1}$$

TABLE III. DFT calculated magnetic interaction parameters in units of meV of the general bilinear exchange Hamiltonian, Eq. (1) in the case of $U = 2.5$ and 3.5 eV.

	J Path		d (Å)	J	K	Γ^x	Γ^y	Γ^z	D^x	D^y	D^z
$U = 2.5$	NN	x/y	3.129	1.60	−10.73	−1.14	1.14	−1.29	0	0	0
		z	3.138	2.48	−12.42	−0.83	−0.97	0.70	0	0	0
	NNN	x/y	5.425	0.08	− 0.18	− 0.02	0.07	0.05	− 0.12	− 0.15	− 0.05
		z	5.427	0.20	− 0.22	0.05	0.07	0.15	0.21	0.07	0.17
	NNNN	z	6.257	1.02	0.15	0.01	0.01	0.07	− 0.02	0.02	0.00
		x/y	6.269	1.03	0.15	0.07	0.01	0.01	− 0.01	− 0.01	0.02
	J Path		d (Å)	J	K	Γ^x	Γ^y	Γ^z	D^x	D^y	D^z
$U = 3.5$	NN	x/y	3.129	1.13	− 8.50	− 0.97	0.90	− 1.10	0	0	0
		z	3.138	1.86	− 9.78	− 0.71	− 0.83	0.69	0	0	0
	NNN	x/y	5.425	0.07	− 0.11	− 0.00	0.06	0.03	− 0.08	− 0.11	− 0.02
		z	5.427	0.13	− 0.12	0.04	0.05	0.10	0.13	0.04	0.12
	NNNN	z	6.257	0.66	0.13	0.01	0.01	0.07	− 0.01	0.01	0.00
		x/y	6.269	0.68	0.12	0.06	0.01	0.02	− 0.00	− 0.00	0.01

In Eq. (C1), all elements are 3-by-3 matrices. The nonvanishing matrices are

$$H_{12} = \frac{1}{2}\begin{bmatrix} J_1 & \Gamma_1 & -\Gamma_1 \\ \Gamma_1 & J_1 & -\Gamma_1 \\ -\Gamma_1 & -\Gamma_1 & J_1 + K_1 \end{bmatrix} e^{2\pi i k_y} + \frac{1}{2} J_3 [1 + 2\cos(2\pi k_x) e^{2\pi i k_y}] E_{3\times 3}, \quad \text{(C2)}$$

$$H_{14} = \frac{1}{2}\begin{bmatrix} J_1 & -\Gamma_1 & \Gamma_1 \\ -\Gamma_1 & J_1 + K_1 & -\Gamma_1 \\ \Gamma_1 & -\Gamma_1 & J_1 \end{bmatrix} + \frac{1}{2}\begin{bmatrix} J_1 + K_1 & -\Gamma_1 & -\Gamma_1 \\ -\Gamma_1 & J_1 & \Gamma_1 \\ -\Gamma_1 & \Gamma_1 & J_1 \end{bmatrix} e^{2\pi i k_x}, \quad \text{(C3)}$$

$$H_{23} = \frac{1}{2}\begin{bmatrix} J_1 & -\Gamma_1 & \Gamma_1 \\ -\Gamma_1 & J_1 + K_1 & -\Gamma_1 \\ \Gamma_1 & -\Gamma_1 & J_1 \end{bmatrix} e^{2\pi i k_x} + \frac{1}{2}\begin{bmatrix} J_1 + K_1 & -\Gamma_1 & -\Gamma_1 \\ -\Gamma_1 & J_1 & \Gamma_1 \\ -\Gamma_1 & \Gamma_1 & J_1 \end{bmatrix}, \quad \text{(C4)}$$

$$H_{34} = \frac{1}{2}\begin{bmatrix} J_1 & \Gamma_1 & -\Gamma_1 \\ \Gamma_1 & J_1 & -\Gamma_1 \\ -\Gamma_1 & -\Gamma_1 & J_1 + K_1 \end{bmatrix} + \frac{1}{2} J_3 [e^{2\pi i k_y} + 2\cos(2\pi k_x)] E_{3\times 3}. \quad \text{(C5)}$$

In Eqs. (C2) and (C5), $E_{3\times 3}$ is a 3-by-3 unit matrix. Here we set the lattice constants $\boldsymbol{a}$ and $\boldsymbol{b}$ to be unit, and (k_x, k_y) is a point in momentum space. The parameters J_1, K_1, Γ_1, and J_3 are the magnetic interaction parameters of the minimal J_1-K_1-Γ_1-J_3 model [see Eq. (6) in the main text].

APPENDIX D: DEPENDENCE OF EXCHANGE PARAMETERS OF Na_2Ir_3 ON THE ON-SITE COULOMB ENERGY U

We show the dependence of exchange parameters of Na_2Ir_3 on the on-site U. From Tables I and III, one can obtain that, although the magnitudes of the exchange parameters vary as the Coulomb energy on-site U changes, the relative strengths between the NN, NNN, and NNNN exchange parameters have slight variations. All in all, the third-NN Heisenberg interactions are sizable, whereas the second-NN magnetic interactions are extremely weak compared with the NN interactions.

[1] J. G. Rau, E. K. H. Lee, and H. Y. Kee, Annu. Rev. Condens. Matter Phys. **7**, 195 (2016).
[2] D. Pesin and L. Balents, Nat. Phys. **6**, 376 (2010).
[3] X. G. Wan, A. M. Turner, A. Vishwanath, and S. Y. Savrasov, Phys. Rev. B **83**, 205101 (2011).
[4] Y. J. Yan, M. Q. Ren, H. C. Xu, B. P. Xie, R. Tao, H. Y. Choi, N. Lee, Y. J. Choi, T. Zhang, and D. L. Feng, Phys. Rev. X **5**, 041018 (2015).
[5] H. Watanabe, T. Shirakawa, and S. Yunoki, Phys. Rev. Lett. **110**, 027002 (2013).
[6] G. Jackeli and G. Khaliullin, Phys. Rev. Lett. **102**, 017205 (2009).
[7] J. Chaloupka, G. Jackeli, and G. Khaliullin, Phys. Rev. Lett. **105**, 027204 (2010).
[8] A. Kitaev, Ann. Phys. (N.Y.) **321**, 2 (2006).
[9] X. Liu, T. Berlijn, W. G. Yin, W. Ku, A. Tsvelik, Y.-J. Kim, H. Gretarsson, Y. Singh, P. Gegenwart, and J. P. Hill, Phys. Rev. B **83**, 220403 (2011).
[10] F. Ye, S. Chi, H. Cao, B. C. Chakoumakos, J. A. Fernandez-Baca, R. Custelcean, T. F. Qi, O. B. Korneta, and G. Cao, Phys. Rev. B **85**, 180403 (2012).
[11] S. K. Choi, R. Coldea, A. N. Kolmogorov, T. Lancaster, I. I. Mazin, S. J. Blundell, P. G. Radaelli, Y. Singh, P. Gegenwart, K. R. Choi, S. W. Cheong, P. J. Baker, C. Stock, and J. Taylor, Phys. Rev. Lett. **108**, 127204 (2012).
[12] Y. Singh, S. Manni, J. Reuther, T. Berlijn, R. Thomale, W. Ku, S. Trebst, and P. Gegenwart, Phys. Rev. Lett. **108**, 127203 (2012).

[13] K. Mehlawat, G. Sharma, and Y. Singh, Phys. Rev. B **92**, 134412 (2015).
[14] S. H. Chun, J.-W. Kim, J. Kim, H. Zheng, C. C. Stoumpos, C. D. Malliakas, J. F. Mitchell, K. Mehlawat, Y. Singh, Y. Choi, T. Gog, A. Al-Zein, M. M. Sala, M. Krisch, J. Chaloupka, G. Jackeli, G. Khaliullin, and B. J. Kim, Nat. Phys. **11**, 462 (2015).
[15] R. Comin, G. Levy, B. Ludbrook, Z. H. Zhu, C. N. Veenstra, J. A. Rosen, Y. Singh, P. Gegenwart, D. Stricker, J. N. Hancock, D. van der Marel, I. S. Elfimov, and A. Damascelli, Phys. Rev. Lett. **109**, 266406 (2012).
[16] I. Kimchi and A. Vishwanath, Phys. Rev. B **89**, 014414 (2014).
[17] J. G. Rau, E. K.-H. Lee, and H.-Y. Kee, Phys. Rev. Lett. **112**, 077204 (2014).
[18] I. Kimchi and Y.-Z. You, Phys. Rev. B **84**, 180407 (2011).
[19] Y. Sizyuk, C. Price, P. Wölfle, and N. B. Perkins, Phys. Rev. B **90**, 155126 (2014).
[20] S. M. Winter, Y. Li, H. O. Jeschke, and R. Valenti, Phys. Rev. B **93**, 214431 (2016).
[21] J. Chaloupka, G. Jackeli, and G. Khaliullin, Phys. Rev. Lett. **110**, 097204 (2013).
[22] V. M. Katukuri, S. Nishimoto, V. Yushankhai, A. Stoyanova, H. Kandpal, S. Choi, R. Coldea, I. Rousochatzakis, L. Hozoi, and J. van den Brink, New J. Phys. **16**, 013056 (2014).
[23] Y. Yamaji, Y. Nomura, M. Kurita, R. Arita, and M. Imada, Phys. Rev. Lett. **113**, 107201 (2014).
[24] K. Hu, F. Wang, and J. Feng, Phys. Rev. Lett. **115**, 167204 (2015).
[25] K. Foyevtsova, H. O. Jeschke, I. I. Mazin, D. I. Khomskii, and R. Valentí, Phys. Rev. B **88**, 035107 (2013).
[26] B. J. Kim, H. Jin, S. J. Moon, J. Y. Kim, B. G. Park, C. S. Leem, J. Yu, T. W. Noh, C. Kim, S. J. Oh, J. H. Park, V. Durairaj, G. Cao, and E. Rotenberg, Phys. Rev. Lett. **101**, 076402 (2008).
[27] Y. S. Hou, H. J. Xiang, and X. G. Gong, Phys. Rev. B **96**, 054410 (2017).
[28] J. P. Perdew, K. Burke, and M. Ernzerhof, Phys. Rev. Lett. **77**, 3865 (1996).
[29] P. E. Blochl, Phys. Rev. B **50**, 17953 (1994).
[30] A. I. Liechtenstein, V. I. Anisimov, and J. Zaanen, Phys. Rev. B **52**, R5467 (1995).
[31] N. Marzari and D. Vanderbilt, Phys. Rev. B **56**, 12847 (1997).
[32] I. Souza, N. Marzari, and D. Vanderbilt, Phys. Rev. B **65**, 035109 (2001).
[33] A. A. Mostofi, J. R. Yates, Y. S. Lee, I. Souza, D. Vanderbilt, and N. Marzari, Comput. Phys. Commun. **178**, 685 (2008).
[34] K. Hukushima and K. Nemoto, J. Phys. Soc. Jpn. **65**, 1604 (1996).
[35] Y. S. Hou, H. J. Xiang, and X. G. Gong, New J. Phys. **18**, 043007 (2016).
[36] P. S. Wang, W. Ren, L. Bellaiche, and H. J. Xiang, Phys. Rev. Lett. **114**, 147204 (2015).
[37] B. H. Kim, T. Shirakawa, and S. Yunoki, Phys. Rev. Lett. **117**, 187201 (2016).
[38] T. Okubo, K. Shinjo, Y. Yamaji, N. Kawashima, S. Sota, T. Tohyama, and M. Imada, Phys. Rev. B **96**, 054434 (2017).
[39] H.-S. Kim, V. Vijay Shankar, A. Catuneanu, and H.-Y. Kee, Phys. Rev. B **91**, 241110 (2015).
[40] H. J. Xiang, E. J. Kan, S. H. Wei, M. H. Whangbo, and X. G. Gong, Phys. Rev. B **84**, 224429 (2011).
[41] Since there is no concept of $J_{\text{eff}} = 1/2$ states in the original WANNIER90 and VASP, we define the projector of Wannier orbitals of $J_{\text{eff}} = 1/2$ states based on Eqs. (2a) and (2b). This procedure is similar to obtaining the $sp3$ hybridization Wannier orbital, which has been well implemented in WANNIER90 and VASP. Note that SOC has to be included to get $J_{\text{eff}} = 1/2$ Wannier orbitals.
[42] H.-S. Kim, C. H. Kim, H. Jeong, H. Jin, and J. Yu, Phys. Rev. B **87**, 165117 (2013).
[43] T. Micklitz and M. R. Norman, Phys. Rev. B **81**, 174417 (2010).
[44] S. M. Winter, K. Riedl, P. A. Maksimov, A. L. Chernyshev, A. Honecker, and R. Valenti, Nat. Commun. **8**, 1152 (2017).
[45] T. Suzuki, T. Yamada, Y. Yamaji, and S.-i. Suga, Phys. Rev. B **92**, 184411 (2015).
[46] E. Dagotto, Rev. Mod. Phys. **66**, 763 (1994).
[47] E. R. Gagliano and C. A. Balseiro, Phys. Rev. Lett. **59**, 2999 (1987).
[48] T. Takayama, A. Kato, R. Dinnebier, J. Nuss, H. Kono, L. S. I. Veiga, G. Fabbris, D. Haskel, and H. Takagi, Phys. Rev. Lett. **114**, 077202 (2015).
[49] A. Biffin, R. D. Johnson, I. Kimchi, R. Morris, A. Bombardi, J. G. Analytis, A. Vishwanath, and R. Coldea, Phys. Rev. Lett. **113**, 197201 (2014).